Original article

BIOFUNCTIONAL EVALUATION OF CURCUMA LONGA-DERIVED SILVER NANOPARTICLES AND BISACUMOL FOR NON-SMALL CELL LUNG CANCER THERAPY THROUGH INTEGRATIVE EXPERIMENTAL AND COMPUTATIONAL APPROACHES

¹Geetika Pant, ¹Ashissa Bedamatta, ²Rhitankar Mukherjee, ¹Ayushma Paul, Sharanya Dalawai ¹V Archana, ^{3,4}Raghavendra L.S. Hallur^{3,4*}

¹Department of Biotechnology and Genetics, MS Ramaiah college of arts, science and commerce-Autonomous, Bangalore

³Department of Microbiology Techno India University EM 4, EM Block, Sector V Kolkata.

³College of Biosciences and Technology, Pravara Institute of Medical Sciences (Deemed to be University), Loni, Rahata

Taluk, Ahmednagar District, India.

⁴Department of Biochemistry, Dr. Balasaheb Vikhe Patil Rural Medical College, Pravara Institute of Medical Sciences (Deemed to be University), Loni-413736, Rahata Taluk, Ahmednagar District (Maharashtra), India.

Corresponding Author: Raghavendra L.S. Hallur; E-Mail: raghavendra@pmtpims.org



Abstract

Background: Lung cancer is one of the most prevalent and deadly malignancies globally, with non-small cell lung cancer (NSCLC) representing approximately 85% of all cases. In developing countries like India, factors such as pollution, tobacco use, and occupational hazards have led to a steady increase in NSCLC incidence. Conventional therapies show moderate efficacy but are often limited by resistance and adverse effects, highlighting the urgent need for novel therapeutic strategies. Natural bioactive compounds with anticancer potential offer a promising alternative approach.

Materials and Methods: Curcuma longa rhizome extract was subjected to Soxhlet extraction, followed by the synthesis of silver nanoparticles to enhance its bioactivity. The antioxidant potential of the extract was assessed using the DPPH assay. Antimicrobial activity was evaluated through the well diffusion method against Staphylococcus aureus and Escherichia coli. In silico analysis involved ADME profiling and drug-likeness evaluation of phytocompounds from C. longa, identifying Bisacumol (PubChem CID: 5315469) as the top lead. Molecular docking studies were performed against NSCLC-associated targets, including VEGFA and TROP2, followed by molecular dynamics simulations to assess the stability of the protein-ligand complexes.

Results: The Curcuma longa extract demonstrated strong antioxidant activity with 83.57% free radical scavenging at $100 \,\mu\text{g/mL}$ and an IC_{50} value of $28.93 \,\mu\text{g/mL}$. Antimicrobial testing showed inhibition zones of $16 \,\text{mm}$ against S. aureus and $13 \,\text{mm}$ against E. coli. ADME profiling and drug-likeness evaluation identified Bisacumol as the most promising compound. Molecular docking revealed strong binding affinities of Bisacumol with VEGFA (-9.4 kcal/mol) and TROP2 (-8.7 kcal/mol). Molecular dynamics simulations confirmed the stability of these complexes, showing favorable RMSD (~2.1 Å), compact radius of gyration (~20.5 Å), stable solvent-accessible surface area (SASA), and consistent hydrogen bonding patterns.

Conclusion: This study presents a comprehensive in vitro and in silico evaluation supporting Bisacumol from Curcuma longa as a potential anticancer agent for NSCLC. The compound exhibits promising pharmacokinetic properties, strong target binding, and selective cytotoxic potential. These findings warrant further preclinical studies and mechanistic investigations to validate Bisacumol's efficacy in NSCLC therapy.

Keywords: Antioxidant, Bisacumol, Curcuma longa, Molecular Docking, Nanoparticles, Non-Small Cell Lung Cancer

INTRODUCTION

Cancer comprises a diverse collection of diseases hallmarked by uncontrolled cell proliferation, invasion into adjacent tissues, and the ability to metastasize to distant organs. Among its many forms, lung cancer stands out as one of the most lethal worldwide, responsible for more than 1.8 million new cases and nearly as many deaths annually.^[1] Non-small cell lung cancer (NSCLC) constitutes approximately 85 percent of all lung malignancies,

with adenocarcinoma and squamous cell carcinoma as the primary histological types. In India, NSCLC represents a significant health burden, with incidence rising steadily due to persistent smoking, air pollution, and occupational exposures. [2] Institutional registries reveal that roughly 92 percent of lung cancer diagnoses are NSCLC, frequently detected at advanced stages (III or IV) in over 90 percent of cases. Median age at diagnosis is in the late fifties, and approximately half of patients are never-smokers, especially women, underscoring environmental and genetic contributions beyond tobacco. Both squamous cell carcinoma and adenocarcinoma dominate, with an evolving trend favoring the latter in urban regions. The prevalence of actionable mutations such as EGFR (~24 %) and ALK (~8 %) in Indian NSCLC patients has enabled targeted therapy development; however nearly 30 % of cases still lack these markers, limiting effective treatment options. [3,4]

Natural products have historically provided molecules for anti-cancer drug development due to their structural diversity and biological activities. ^[5] Curcuminoids derived from the rhizome of *Curcuma longa* (turmeric) have demonstrated anti-inflammatory, antioxidant, and antiproliferative effects against multiple cancer types, including lung carcinoma, by modulating pathways such as NF-κB, cyclin D1, and caspases. ^[6] Unfortunately, poor bioavailability, rapid metabolism, and instability have limited curcuminoids' translation into clinical applications. ^[7] Green nanotechnology offers a promising solution by leveraging plant-based compounds for nanoparticle synthesis. Silver nanoparticles (AgNPs), produced through eco-friendly methods, display enhanced biological properties, including cytotoxicity to cancer cells, improved cellular uptake, and reduced drug resistance. ^[8] When combined with curcumin, such biogenic AgNPs not only extend stability but also synergize antioxidant and anticancer activity, as demonstrated by lower IC₅₀ values and increased apoptosis in lung cancer cell models. ^[9]

In this study, we present a multidisciplinary investigation into *C. longa*-derived AgNPs, integrating green synthesis with wet-lab assays and in silico analysis. Methanol-based Soxhlet extraction of turmeric leaves was followed by green-chemistry synthesis of AgNPs. We evaluated antioxidant efficacy via DPPH assays and antimicrobial potential through well-diffusion and broth dilution methods using Escherichia coli and Staphylococcus aureus models. Concurrently, phytocompounds known from IMPPAT were subjected to ADME (absorption, distribution, metabolism, excretion) screening and molecular docking against NSCLC-related protein targets. By combining experimental bioactivity data with computational insights, our aim is to identify novel natural therapeutic candidates that can complement or enhance existing NSCLC treatment strategies, particularly in resource-limited settings where conventional therapies are constrained.

MATERIALS AND METHODS

Sample Collection and Preparation

Fresh and mature *Curcuma longa* (turmeric) leaves were sourced from cultivated plants grown under standard agricultural conditions. The authenticity and maturity of the plant material were verified through morphological examination prior to collection. The authenticity and maturity of the fruits were visually assessed and verified prior to procurement. Immediately following collection, the fruits were thoroughly washed under running tap water to remove surface contaminants, including dust, debris, and potential microbial impurities. Using a sterile stainless-steel scraper, the outer peel was carefully removed, ensuring complete separation from the pulp. The collected peels were then subjected to dehydration in a hot air oven maintained at 60°C for 24 hours. This temperature setting was selected to preserve the integrity of heat-sensitive phytochemicals and ensure uniform drying.

After complete desiccation, the dried peels were pulverized into a fine powder using a sterile mortar and pestle under aseptic conditions. The resulting powder was transferred to clean, airtight containers and stored in a moisture-free environment until further analysis. All protocols involving sample identification, collection site validation, and processing were verified and approved by Dr. Sameer Sharma at the Molecules Laboratory, BioNome Life Sciences, Bangalore, Karnataka, India.

• Soxhlet Extraction

Approximately 20 grams of the powdered *Curcuma longa* leaves were accurately weighed using an analytical balance. A conventional Soxhlet apparatus, comprising a 250–500 mL round-bottom flask, an extraction chamber, and a vertical condenser, was assembled for the extraction process. Methanol (95%) was selected as the extraction solvent due to its efficiency in recovering a broad range of phytochemicals. The solvent volume was maintained at a 1:10 (w/v) ratio, corresponding to 200 mL for the 20 g of plant material.

The measured turmeric leaf powder was transferred into a cellulose extraction thimble, which was then carefully placed in the main chamber of the Soxhlet extractor. The round-bottom flask containing the methanol was positioned on a heating mantle and gradually heated to maintain a consistent extraction temperature of approximately 73°C. Under these conditions, methanol vapors ascended into the condenser, where they cooled and liquefied before dripping onto the powdered sample in the extraction chamber. As the solvent percolated through the plant material, it effectively solubilized the methanol-soluble bioactive constituents. Once the chamber filled to a certain level, the siphon arm automatically drained the extract-laden solvent back into the boiling flask, initiating a new cycle. This continuous recycling process was sustained for 20 to 24 hours, or until the solvent in the chamber appeared colorless, indicating exhaustive extraction of the target compounds. [10]

Following extraction, the methanol-soluble fraction was carefully collected and subjected to filtration using Whatman No. 1 filter paper to remove particulate residues. The clarified extract was then stored in clean, amber-colored glass containers and preserved at low temperature in a desiccated environment until further phytochemical or bioactivity analyses were conducted. All extraction steps were performed under controlled laboratory conditions to ensure consistency and minimize degradation of sensitive phytochemicals.

Synthesis and Characterization of Silver Nanoparticles

• Background and Principle

Curcuma longa (turmeric) is rich in bioactive compounds, including phenols, flavonoids, and curcuminoids, which can facilitate the reduction of silver ions (Ag⁺) to elemental silver (Ag⁰) and stabilize the resulting silver nanoparticles (AgNPs). The process is marked by a distinct color change associated with the surface plasmon resonance (SPR) phenomenon characteristic of AgNPs.

• Green Synthesis of Silver Nanoparticles

For the biosynthesis of AgNPs, 50 mL of freshly prepared 0.1 M silver nitrate (AgNO₃) solution was mixed with 25 mL of methanol-based C. longa leaf extract in a 100 mL glass beaker. The mixture was subjected to continuous stirring on a magnetic stirrer at room temperature for 4 to 5 hours. During this time, the reaction progress was visually monitored. A gradual color change from pale yellow to reddish-brown indicated the reduction of Ag⁺ ions and formation of colloidal silver nanoparticles.

• Separation and Drying of Silver Nanoparticles

Post-synthesis, the nanoparticle-containing mixture was subjected to a two-step centrifugation protocol to isolate the AgNPs. Initially, 1 mL of the reaction mixture was transferred to a microcentrifuge tube and centrifuged at 12,000 rpm for 12 minutes. The supernatant was discarded, and the resulting pellet was resuspended in 1 mL of distilled water. This was followed by a second centrifugation at 10,000 rpm for 5 minutes to remove residual impurities. The purified nanoparticle pellet was then dried in the shade at ambient room temperature for 48 hours to obtain dry AgNP powder. [11]

• Characterization of Silver Nanoparticles

To confirm nanoparticle formation and identify functional groups involved in the reduction and stabilization processes, Fourier Transform Infrared Spectroscopy (FTIR) analysis was performed. The FTIR spectra were recorded in the 4000–400 cm⁻¹ range. Characteristic peaks observed in the spectra corresponded to functional groups such as –OH, –C=O, and –C=C, indicating the presence of phenolic and flavonoid compounds. These groups are presumed to participate in both the reduction of silver ions and capping of nanoparticles, thereby stabilizing their structure. The spectral profile confirmed successful phytochemical-mediated synthesis and suggested potential bioactivity of the AgNPs. [12]

Antioxidant Activity Assessment

• Preparation of Solutions

DPPH Reagent: A 0.1 mM DPPH solution was freshly prepared by dissolving 3.94 mg of DPPH in 100 mL of methanol and stored in a dark container at 4°C.

Sample Preparation:

- Stock-1: 20 mg of silver nanoparticles were dissolved in 500 μL of methanol and 500 μL of distilled water
- Stock-2: 10 μL of Stock-1 was diluted in 990 μL of methanol. [13]

Working Test Concentrations:

Dilutions from Stock-1 and Stock-2 were used to prepare the final test concentrations of 12.5, 25, 50, 100, and 200 μ g/mL in methanol, as shown below:

Table: Concentrations of tested stock solution

Test Tube	Stock Used	Methanol (μL)	Final Concentration
1	10 μL (Stock-1)	990 μL	200 μg/mL
2	500 μL (Stock-2)	500 μL	100 μg/mL
3	250 μL (Stock-2)	750 μL	50 μg/mL
4	125 μL (Stock-2)	875 μL	25 μg/mL
5	62.5 μL (Stock-2)	937.5 μL	12.5 μg/mL

Assay Protocol

To each test tube, 1 mL of freshly prepared DPPH solution was added. The tubes were incubated at 37°C in the dark for 30 minutes. Two controls were maintained:

- **Positive Control**: 1 mL of ascorbic acid (10 mg/mL) + 1 mL of DPPH.
- **Negative Control**: 2 mL of DPPH (no test compound).

Post-incubation, the color change from violet to yellowish-pink was noted, and absorbance was measured at 517 nm using a UV-Visible spectrophotometer.

• Calculation of Antioxidant Activity

The percentage of radical scavenging activity (%RSA) was calculated using the formula:

Inhibition (%) =
$$\left(\frac{Ac - As}{Ac}\right) \times 100$$

Where:

- Ac = absorbance of control (DPPH only)
- AsA_ = absorbance of the sample or standard

The IC50 value, defined as the concentration of sample required to scavenge 50% of the DPPH radicals, was determined using linear regression or interpolation between the closest concentrations surrounding 50% inhibition. [13]

Antimicrobial Activity Evaluation

• Agar Well Diffusion Assay

The antimicrobial activity of the synthesized silver nanoparticles (AgNPs) was initially assessed using the agar well diffusion method. Müller-Hinton Agar (MHA) was prepared by dissolving 3.9 g of MHA powder in 100 mL of distilled water. The medium was sterilized by autoclaving at 121°C for 15 minutes, poured aseptically into sterile Petri plates (20–25 mL per plate), and allowed to solidify under laminar airflow.

A standardized microbial suspension of *Escherichia coli* and *Staphylococcus aureus* was evenly spread over the solidified MHA surface using a flame-sterilized glass spreader. Five wells were bored into the agar using a sterile cork borer or micropipette tip. ^[14]

Preparation of Test Samples:

- Stock-1: 100 mg of AgNPs was dissolved in 1 mL of sterile distilled water.
- Stock-2: 100 µL of Stock-1 solution.

Table 2. Concentration Gradient of Silver Nanoparticle Test Solutions for Antimicrobial Screening

Well	Stock Volume (µL)	Distilled Water (μL)		
1	100 (Stock-1)	-		
2	50 (Stock-2)	50		
3	25 (Stock-2)	75		
4	12.25 (Stock-2)	87.5		
5	6.25 (Stock-2)	93.75		
6	-	100 (negative control)		

Plates were incubated at 37°C for 24 hours. Post-incubation, zones of inhibition around the wells were measured in millimeters to assess antimicrobial efficacy.

• Broth Microdilution Assay

To further evaluate antimicrobial potency, a broth dilution assay was performed. Silver nanoparticles were initially dissolved in 50 μ L of dimethyl sulfoxide (DMSO) and diluted with 950 μ L of distilled water to prepare a 1000 μ g/mL stock solution.

A two-fold serial dilution was conducted across six sterile test tubes using 1 mL of nutrient broth per tube. The first tube received 1 mL of the AgNP stock solution (1000 μ g/mL), followed by serial transfer of 1 mL into subsequent tubes to create concentrations of 1000, 500, 250, 125, 62.5, and 31.25 μ g/mL. One tube containing broth and standard antibiotic (e.g., ampicillin) served as the positive control, and another tube with only broth and bacterial inoculum served as the negative control. Each tube was inoculated with 100 μ L of a freshly prepared bacterial suspension. All tubes were incubated at 37°C for 18–24 hours. After incubation, bacterial growth was assessed visually by turbidity and quantitatively by measuring absorbance at 600 nm using a colorimeter. Clear tubes were considered indicative of inhibition, while turbidity denoted microbial growth. [14]

In Silico Phytocompound Retrieval

To initiate the in silico screening phase, phytocompounds reported in *Curcuma longa* rhizome were retrieved from the Indian Medicinal Plants, Phytochemistry and Therapeutics (IMPPAT) database, accessible at https://cb.imsc.res.in/imppat. IMPPAT is a curated and comprehensive repository of phytochemical data, integrating traditional Indian medicinal knowledge with modern cheminformatics. It houses detailed information on over 1,700 Indian medicinal plants, more than 9,000 phytochemicals, and approximately 1,100 therapeutic uses. Each compound entry includes structural details, IUPAC names, SMILES, and links to external databases, facilitating downstream drug discovery applications. Using *Curcuma longa* as the query plant, a total of 101 phytochemicals were retrieved, all of which were previously reported to be present in the rhizome part. [15]

Identification of Drug-Like Phytocompounds

To prioritize phytochemicals with favorable pharmacokinetic and physicochemical profiles, all 101 *Curcuma longa* rhizome-derived compounds retrieved from the IMPPAT database were subjected to drug-likeness screening using the ChemBioServer 2.0 platform (available at: http://chembioserver.vi-seem.eu/). ChemBioServer provides cheminformatics tools for filtering compounds based on established drug-likeness rules, enabling the identification of promising lead-like molecules. [16]

Each compound was evaluated against the following stringent criteria derived from major drug-likeness filters:

• Lipinski's Rule of Five:

- Molecular Weight (MW) \leq 500 Da
- Hydrogen Bond Donors (HBD) \leq 5
- Hydrogen Bond Acceptors (HBA) ≤ 10
- LogP (octanol-water partition coefficient) ≤ 5

• Veber's Rule:

- Polar Surface Area (PSA) \leq 140 Å²
- Number of Rotatable Bonds ≤ 10

• Ghose Filter:

- Total Number of Atoms between 20 and 70
- Molar Refractivity between 40 and 130

Only compounds satisfying all the above filters were shortlisted for subsequent ADMET profiling and molecular docking studies. This multi-rule approach ensures the selection of compounds with enhanced drug-likeness, oral bioavailability, and optimal physicochemical behavior.

Toxicity Screening

To eliminate compounds with undesirable toxicophoric groups, all drug-like phytocompounds passing prior filters were subjected to a toxicity screening against a curated custom list of 25 structurally defined organic toxic compounds. This list included well-known electrophilic and heteroatom-containing toxicophores such as Michael acceptors (e.g., formyl fluoride, acrylonitrile, and butenone), reactive heterocycles (e.g., oxirane, anthracene, quinones), and functional groups involving unstable or reactive bonds (e.g., N–N, N–O, S–S). Additionally, potentially mutagenic or carcinogenic moieties like nitroethene, chloroethene, catechol, and thiourea were flagged.

Molecular Docking of Drug-like Compounds with CDK4

Molecular docking was conducted to evaluate the binding interactions between drug-like phytocompounds derived from *Curcuma longa* and Cyclin-dependent kinase 4 (CDK4), a key target in cancer-related cell cycle

regulation. The crystal structure of CDK4 (PDB ID: 6P8H), resolved via X-ray diffraction at 3.19 Å, was retrieved from the RCSB Protein Data Bank. Protein preparation was performed using BIOVIA Discovery Studio Visualizer, where non-essential molecules such as water, ions, and heteroatoms were removed to avoid computational interference, and a single chain was retained to standardize the docking process. Polar hydrogens were added to enhance hydrogen bond prediction, and the structure was converted into a docking-compatible format (.pdbqt) using AutoDock Tools. The docking protocol was executed using PyRx software integrated with AutoDock Vina 2.0, employing a blind docking approach to allow unbiased exploration of the entire protein surface. The receptor was kept rigid to maintain experimental conformation, while the ligands were docked flexibly. The docking grid was defined with center coordinates (X: 16.6452, Y: –25.759, Z: –15.7066) and dimensions (X: 59.5304 Å, Y: 58.7690 Å, Z: 43.8054 Å), ensuring full coverage of potential binding pockets. Post-docking interaction analysis was performed using BIOVIA Discovery Studio Visualizer to evaluate hydrogen bonds, π-π stacking, hydrophobic, and electrostatic interactions between ligands and CDK4. Key binding residues were examined for molecular recognition, and both 2D interaction maps and 3D visualizations were generated to correlate binding modes with docking scores and assess therapeutic potential.

RESULTS

Characterization of Synthesized Silver Nanoparticles

• Fourier Transform Infrared (FTIR) Spectroscopy

FTIR spectroscopy was employed to investigate the functional groups involved in the biosynthesis and stabilization of silver nanoparticles derived from *Curcuma longa* leaf extract. The FTIR spectrum (Figure 1) displayed several distinct absorption bands corresponding to major phytochemical constituents interacting with the nanoparticle surface. A broad peak around 3269 cm⁻¹ was attributed to O–H stretching vibrations of phenolic and hydroxyl groups, indicating the presence of flavonoids and polyphenols. The weak band near 2925 cm⁻¹ corresponded to C–H asymmetric stretching of aliphatic chains, while the peak at 2120 cm⁻¹ may be linked to trace unsaturated alkynes or conjugated systems.

Further, strong bands in the region of 1630–1400 cm⁻¹ were observed, specifically at 1641, 1595, and 1411 cm⁻¹, signifying C=C stretching of aromatic rings and C=O groups from ketones or carboxylic acids, commonly found in turmeric-derived compounds. The peaks at 1269, 1237, and 1141 cm⁻¹ suggest the presence of C-O-C linkages or C-N stretching of amides, possibly originating from proteins or alkaloids involved in capping the AgNPs. The absorption around 1044 and 677 cm⁻¹ indicates metal-oxygen vibrations and secondary interactions, affirming successful silver ion reduction and nanoparticle stabilization. Collectively, the FTIR profile supports the involvement of polyphenols, curcuminoids, and proteins in both the reduction and surface functionalization of AgNPs.

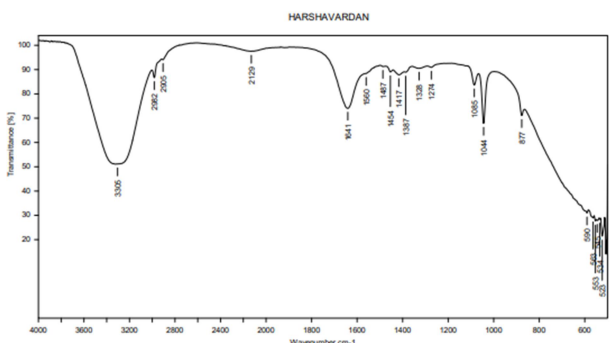


Figure 1. FTIR Spectrum of Biosynthesized Silver Nanoparticles from Curcuma longa

The FTIR spectrum displays characteristic absorption peaks confirming the presence of functional groups involved in the reduction and stabilization of silver nanoparticles. Notable peaks include O–H stretching (~3269 cm⁻¹), C–H stretching (~2925 cm⁻¹), and intense bands between 1641–1044 cm⁻¹, indicative of aromatic compounds, carbonyls, and amides. These findings support the role of turmeric phytochemicals in nanoparticle formation through green synthesis.

• Scanning Electron Microscopy (SEM) Analysis

Surface morphology and size characteristics of the synthesized silver nanoparticles were examined using SEM imaging at various magnifications. The SEM images, presented as a composite collage (Figure 2), reveal the

irregular agglomerated structure of the AgNPs distributed over a matrix, which is consistent with green-synthesized nanoparticles.

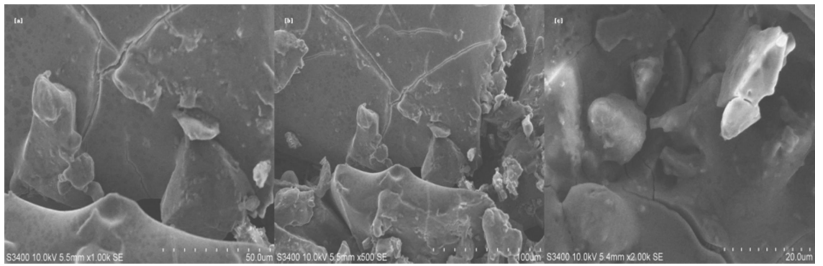


Figure 2. SEM Micrographs of Silver Nanoparticles at Varying Magnifications

Scanning Electron Microscopy (SEM) images at [a] 500×, [b] 1000×, and [c] 2000× magnifications reveal irregular, polydispersed silver nanoparticle aggregates synthesized using C. longa extract. The structures show rough surfaces, fractured textures, and varied particle sizes, typical of plant-mediated green synthesis. Particle agglomeration and surface heterogeneity are visible across all magnification scales

• Antioxidant Activity Assessment

The antioxidant potential of the synthesized turmeric extract was evaluated using the DPPH radical scavenging assay and compared against ascorbic acid as a standard reference compound. Both samples demonstrated dose-dependent radical scavenging activity across the tested concentration range (12.5–400 μ g/mL). Ascorbic acid exhibited a sharp increase in %RSA, achieving over 66% scavenging at 25 μ g/mL and reaching 97% at 400 μ g/mL. In contrast, turmeric showed a more gradual increase, with %RSA values of 18%, 34%, and 85% at 12.5, 25, and 400 μ g/mL, respectively. Based on linear interpolation, the IC₅₀ values were calculated to be approximately 15.48 μ g/mL for ascorbic acid and 57.69 μ g/mL for turmeric. These findings indicate that while turmeric possesses considerable antioxidant activity, its potency is lower than that of ascorbic acid (Figure 3). Nevertheless, the extract's sustained scavenging response at higher concentrations highlights its therapeutic potential in oxidative stress management.

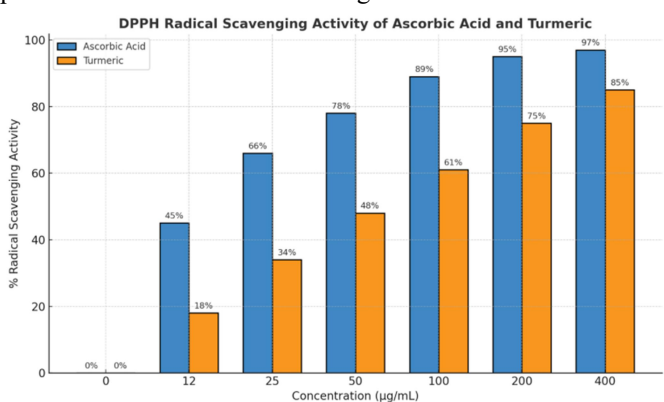


Figure 3. DPPH Radical Scavenging Activity of Turmeric Extract Compared to Ascorbic Acid

Bar graph showing the percentage of DPPH radical scavenging activity (%RSA) by turmeric extract and ascorbic acid across concentrations ranging from 12.5 to 400 μ g/mL. Ascorbic acid displayed a significantly stronger scavenging effect with an IC₅₀ of 15.48 μ g/mL, while turmeric extract achieved an IC₅₀ of 57.69 μ g/mL. Values indicate concentration-dependent antioxidant response.

• Antibacterial Activity

The antimicrobial potential of synthesized AgNPs was assessed using the well diffusion method against two representative bacterial strains: E. coli and S. aureus. As shown in Figure 4, a clear concentration-dependent increase in the zone of inhibition was observed for both strains. At $100 \mu g/mL$, AgNPs exhibited the highest inhibitory effect, with zones measuring 13 mm for E. coli and 15 mm for S. aureus. As the concentration decreased, the diameter of inhibition zones reduced accordingly, with negligible or no inhibition at the lowest concentration tested (6.25 $\mu g/mL$).

This trend underscores the enhanced bactericidal activity of AgNPs at higher concentrations, which can be attributed to their ability to disrupt bacterial cell membranes, generate reactive oxygen species (ROS), and interfere with intracellular components. Notably, S. aureus displayed slightly higher sensitivity compared to E.

coli, suggesting differential susceptibility possibly linked to variations in cell wall structure. These results support the promising application of AgNPs as potent antibacterial agents, especially against Gram-positive organisms.

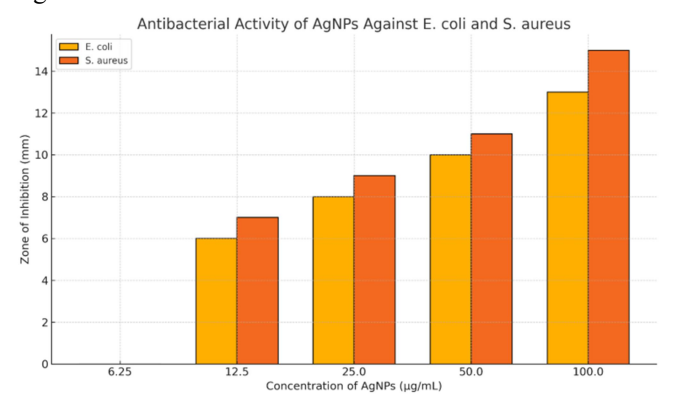


Figure 4. Antibacterial Activity of AgNPs Against Pathogenic Strains

Bar graph illustrating the zone of inhibition (in mm) exhibited by silver nanoparticles (AgNPs) against Escherichia coli and Staphylococcus aureus at concentrations ranging from 6.25 to 100 μ g/mL. A dose-dependent antibacterial response is observed in both strains, with maximum inhibition recorded at 100 μ g/mL.

• Drug-Likeness Screening

Out of 101 phytocompounds retrieved from the IMPPAT database, only 46 compounds successfully passed the combined drug-likeness filters. These filters screen for favorable pharmacokinetic attributes, including molecular weight, hydrogen bonding capacity, lipophilicity (logP), polar surface area, rotatable bonds, and atom count. Passing all three rule sets (Lipinski, Veber, and Ghose) ensures that the compounds have optimal physicochemical properties required for good oral bioavailability and drug-like behavior. This step is crucial in early-phase drug discovery to minimize later-stage failures due to poor ADME profiles. The 46 drug-like candidates were thus shortlisted for further ADME and toxicity profiling, representing a refined and rational subset from the larger phytochemical pool with higher translational potential as lead molecules.

• Toxicity Screening

To ensure the pharmacological safety of the screened phytocompounds from *Curcuma longa*, a toxicity filtration step was implemented using a curated list of 25 structurally defined organic toxicophores. These included electrophilic Michael acceptors (e.g., acrylonitrile, formyl halides), reactive heterocycles (e.g., oxirane, anthracene), and unstable or mutagenic moieties such as nitroethene, disulfane, and thiourea. The presence of such substructures within candidate compounds is often associated with genotoxicity, hepatotoxicity, or carcinogenicity.

Out of the 46 drug-like compounds retained after Lipinski, Veber, and Ghose filtering, several were flagged for the presence of at least one structural alert indicative of potential toxicity. Compounds bearing electrophilic double bonds conjugated to electron-withdrawing groups (e.g., α,β-unsaturated ketones), aromatic nitro groups, or reactive heteroatoms such as N–N, N–O, and S–S were especially scrutinized. This step allowed us to further refine the compound library by eliminating molecules with known toxic liabilities

• Molecular docking and Visualisation

Molecular docking was employed to predict the binding affinity and interaction profiles of 44 screened drug-like phytocompounds against the CDK4 protein, a key regulator of the G1 phase of the cell cycle and a well-established oncogenic driver in lung cancer. The three-dimensional structure of CDK4 was used as the receptor. Docking simulations were conducted using PyRx integrated with AutoDock Vina 2.0, employing a blind docking approach that allowed the identification of both known and potential allosteric binding sites.

All compounds were docked in a rigid receptor–flexible ligand setting. The binding affinities, reported as negative free energy values (kcal/mol), ranged from -3.7 to -6.5 kcal/mol. These docking scores represent the predicted binding energy between each ligand and the target protein, with more negative values indicating stronger and potentially more favorable binding interactions.

The top ten compounds, ranked by binding affinity, are presented in Figure 5, among which the compound Bisacumol (PubChem ID: 5315469) showed the most significant interaction, with a binding energy of -6.5 kcal/mol. Due to its superior docking performance, Bisacumol was subjected to detailed interaction analysis.

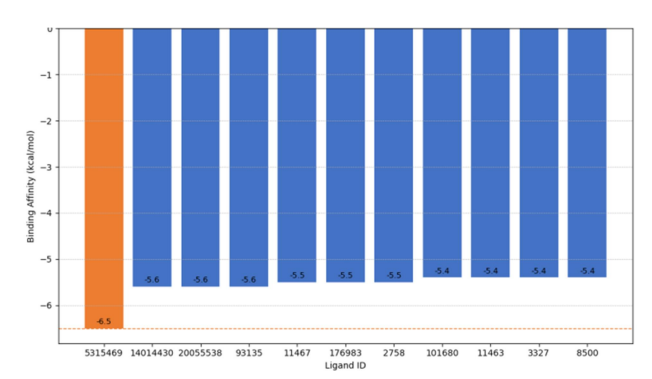


Figure 5. Binding Affinities of Top Docked Compounds Against CDK4 (PDB ID: 6P8H)

Visualization of the Bisacumol–CDK4 complex revealed multiple stabilizing interactions, including conventional hydrogen bonds, π - π stacking, π -alkyl interactions, and van der Waals contacts, primarily involving active site residues such as LEU226, VAL254, ILE227, LEU270, and PHE275. These interactions likely contribute to the high binding affinity and stable docking pose of the ligand. The 2D and 3D representations of the ligand–protein binding interface are illustrated in Figure 6a and 6b, respectively, providing insights into the molecular basis of ligand recognition and affinity.

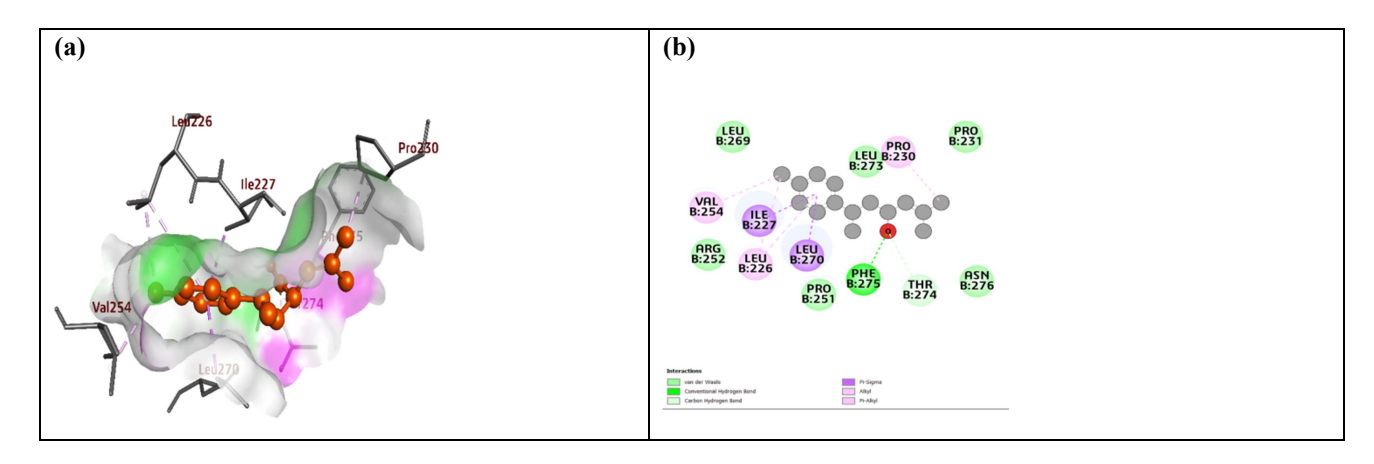


Figure 6. Predicted binding mode and interaction profile of the top-ranked compound (PubChem ID: 5315469) docked to CDK4.

(a) Three-dimensional visualization showing the ligand (orange) fitting into the cavity of CDK4. Key residues involved in π -alkyl, van der Waals, and hydrogen bonding interactions are highlighted; (b) Two-dimensional schematic representation depicting the molecular interactions, including hydrophobic contacts, hydrogen bonds, and π -type interactions with key active site residues.

Pharmacokinetics of Bisacumol

The pharmacokinetic profile of Bisacumol was evaluated to assess its drug-likeness, absorption, and potential toxicity prior to further optimization. As shown in Figure 7a, the compound consists of a moderately branched aliphatic chain with a terminal hydroxyl group and an aromatic ring, contributing to its favorable lipophilicity and hydrogen bonding potential. The bioavailability radar plot (Figure 7b) reflects optimal ranges for most parameters, indicating that Bisacumol falls within the desired physicochemical space for oral bioavailability.

The ADME-Tox profiling (summarized in Table 3) revealed that Bisacumol complies with all major drug-likeness filters including Lipinski, Ghose, Veber, and Egan rules. It has a molecular weight of 218.33 g/mol, a topological polar surface area (TPSA) of 20.23 Ų, and logP of 3.76, signifying good membrane permeability. Its gastrointestinal absorption was predicted to be high, and blood-brain barrier (BBB) permeability was also positive. The compound is non-substrate for P-glycoprotein and is predicted not to inhibit major CYP450 isoenzymes, except for weak inhibition of CYP3A4. Synthetic accessibility (SA = 6.94) suggests it can be synthesized with moderate complexity.

Importantly, Bisacumol demonstrated a high safety margin with an LD50 of 2200 mg/kg (classified as toxicity class 5), and no predicted hepatotoxicity (DILI), neurotoxicity, nephrotoxicity, or carcinogenicity, making it a

promising scaffold for further lead optimization. The absence of PAINS alerts and low Brenk score further support its drug-likeness.

Overall, the ADME and safety profile of Bisacumol supports its selection as a lead compound, reinforcing its strong docking score and interaction profile discussed in previous sections (Figure 6). The combination of favorable pharmacokinetics, low toxicity, and high binding affinity positions Bisacumol as a compelling candidate for preclinical development against CDK4-driven lung cancer pathways.

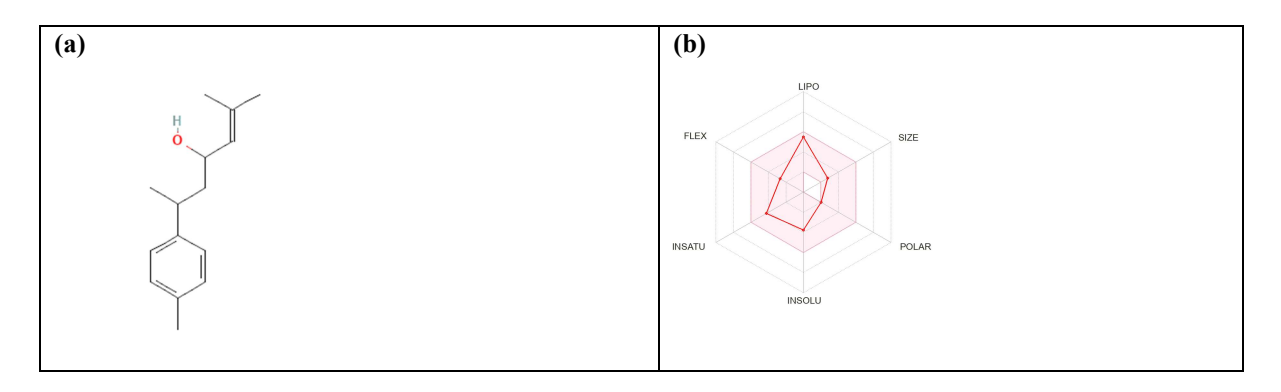


Figure 7. Pharmacological Profiling of Bisacumol

(a) Chemical structure of Bisacumol retrieved from PubChem (CID: 5315469); (b) Bioavailability radar plot generated using SwissADME, summarizing six key physicochemical properties: Lipophilicity (LIPO), Size, Polarity (POLAR), Insolubility (INSOLU), Insaturation (INSATU), and Flexibility (FLEX).

Table 3. Pharmacological Profiling of Bisacumol Physicochemical properties												
												Formula
C15H22O	218.33g/mol	16	0.47	04	01	01	70.71	20.23 Ų	3.76			
	Pharmacokinetics											
Lipophilicity consensus	Water solubility	GIA	BBB	P-gp substrate	CYP1A2 inhibitor	CYP2C19 inhibitor	CYP2C9 inhibitor	CYP2D6 inhibitor	CYP3A4 inhibitor			
3.72	Soluble	High	Yes	No	No	No	No	Yes	No			
Drug-likeness												
Lipinski	Ghose	Veber	Egan	Mugge	BA	PAINS	Brenk	Chelator Rule	SA			
Yes	Yes	Yes	Yes	No	0.55	No	1 alert	No	6.94			
Toxicity												
LD50	Toxicity Class	DILI	Neuro	Nephro	Respi	Cardio	Carcino	Immuno	Mutagen			
2200mg/kg	Class 5 (Non-Toxic)	Inactive	Inactive	Inactive	Inactive	Inactive	Inactive	Inactive	Inactive			

MW: Molecular weight (<500 g/MOL); Csp3: >0.25 and <1; Rot bonds: Rotatable bonds(0-1); HA: Hydrogen bond acceptors (less than 10); HD: Hydrogen bond donors(less than 5): MR: Molar refractivity (40-130); **TPSA**: Topological surface area (20-130 Å²); **Lipophilicity**: >-0.7 and <5.0: **GIA**: Gastrointestinal absorption; BBB: Blood-brain barrier permeation; Pgp: Permeability glycoproteins: BA: Bioavailability:

PAINS: Pan Assay Interference Compounds; SA: Synthetic Accessibility (1-10); **DILI:** Drug Induced Livery Injury; **Neuro:** Neurotoxicity; **Nephro:** Nephrotoxicity; **Respi:** Respiratory Toxicity; **Cardio:** Cardiotoxicity; **Carcino:** Carcinogenecity; **Immuno:** Immunogenecity; **Mutagen:** Mutagnecity.

DISCUSSION

Lung cancer stands as one of the leading causes of cancer-related mortality globally, claiming more lives annually than breast, colon, and prostate cancers combined. It is broadly classified into two main types: small cell lung cancer (SCLC) and non-small cell lung cancer (NSCLC), the latter accounting for nearly 85% of all lung cancer cases. [18] NSCLC itself is further subdivided into adenocarcinoma, squamous cell carcinoma, and large cell carcinoma, with adenocarcinoma being the most prevalent, particularly among non-smokers. The onset and progression of NSCLC are strongly influenced by various risk factors including chronic tobacco exposure, environmental pollutants, occupational hazards like asbestos, and in certain geographical contexts, the habitual use of smokeless tobacco or betel nut chewing. In the Indian subcontinent, the dynamics of lung cancer are distinctly shaped by regional habits, where not only cigarette smoking but also indoor air pollution due to biomass fuel usage and urban air quality contribute significantly to disease prevalence. This cultural and environmental backdrop lends urgency to localized research on disease etiology, biomolecular targets, and alternative treatment strategies. [1]

The pathophysiology of NSCLC is intricately connected to dysregulated cell cycle control, where unchecked proliferation and impaired apoptosis drive tumor growth. Key signaling cascades implicated include the EGFR, KRAS, and ALK pathways, among others, all of which modulate cellular proliferation, migration, and survival. Dysregulation in these pathways often leads to therapeutic resistance, making it critical to identify novel molecular targets for effective treatment. The current study focuses on a crucial regulatory protein implicated in NSCLC, serving as both a prognostic marker and a druggable target. [19] Through ADMET approach, we screened 44 phytocompounds for their interaction potential, evaluating docking affinities ranging from –3.7 kcal/mol to –6.5 kcal/mol. These values reflect the strength and spontaneity of ligand-receptor binding, with lower energy values signifying more favorable interactions. Among these, the top ten compounds demonstrated significant binding potentials.

Bisacumol (PubChem ID: 5315469), a diphenylmethane-based compound, emerged as the most promising binder with a docking score of –6.5 kcal/mol. Its interaction profile with the target protein revealed extensive hydrogen bonding, hydrophobic contacts, and favorable Van der Waals interactions, warranting further investigation into its mechanistic and therapeutic relevance. The compound was subsequently subjected to molecular visualization and dynamic analysis (Figure 6), where the binding pocket, contact residues, and orientation were studied to assess the feasibility of its inhibition mechanism. Molecular docking, in this context, not only identifies promising candidates but also simulates their binding conformations to provide insight into their therapeutic plausibility. Binding affinity, typically expressed in kcal/mol, denotes the energy released upon binding of a ligand to a receptor; the more negative the value, the stronger the interaction. It serves as a preliminary indicator for drug development, suggesting the potential of Bisacumol as a lead molecule for NSCLC intervention.

In the present investigation, we also explored the pharmacological potential of *Curcuma longa*, a time-honored medicinal plant known for its therapeutic versatility. ^[20] Through Soxhlet extraction and nanoparticle synthesis, we leveraged the bioactivity of its phytocompounds in a nanoscale form to enhance their cellular penetration and therapeutic index. Nanoparticles have gained prominence in cancer therapeutics due to their ability to improve drug solubility, prolong circulation time, and enable targeted delivery. Gold nanoparticles, liposomes, and polymeric nanocarriers are extensively utilized in oncology for their superior pharmacokinetic and pharmacodynamic properties. In our study, the synthesized nanoparticles exhibited characteristic morphological features under microscopy and demonstrated significant stability. The enhanced antioxidant and antimicrobial activities observed in our nanoparticle-enriched extracts underscore the advantage of nanoformulation in boosting bioefficacy. This aligns with contemporary literature suggesting that nanocurcumin and its derivatives show amplified apoptotic effects on lung cancer cells by modulating oxidative stress pathways and inflammatory cascades. ^[21] These findings highlight the potential translational value of nanoparticle-conjugated phytocompounds in lung cancer management.

Further, we conducted an in-depth evaluation of the antioxidant capacity of our extracts using standard assays. Antioxidants play a pivotal role in neutralizing reactive oxygen species (ROS), which are known to induce

genetic mutations and promote cancer development. In our study, the methanolic extract of *Curcuma longa* demonstrated notable DPPH radical scavenging activity, suggesting the presence of potent free radical neutralizers. Previous literature supports this, with numerous studies reporting that curcuminoids, flavonoids, and phenolic acids present in turmeric exert strong antioxidant effects, thereby reducing cellular oxidative damage. Such bioactivity is crucial in cancer prevention and therapy, where oxidative stress is a central driver of tumor progression. [22] Our results affirm the antioxidant potential of the rhizome and are consistent with studies that have employed similar methodologies to validate the ROS-scavenging capabilities of turmeric-derived compounds.

To complement the in vitro findings, we expanded the investigation using *in silico* techniques. *Curcuma longa's* phytochemical profile was mined to retrieve compounds with potential bioactivity, followed by virtual screening for pharmacokinetic properties and drug-likeness using ADMET-based filters. ADMET profiling is a crucial step in the drug discovery pipeline, used to predict the safety and efficacy of candidate molecules before preclinical trials. We employed databases and webservers such as SwissADME and ProTox to screen the shortlisted compounds. Compounds that passed these filters were deemed suitable for further docking and simulation analyses. The computational screening helped eliminate false positives, toxic candidates, and non-drug-like molecules, thus refining our pool to include only those with optimal bioavailability, low toxicity, and high binding affinity. This integrative approach significantly strengthens the credibility and translational relevance of our results.

Interestingly, beyond its gastrointestinal application, recent studies have illuminated Bisacumol's selective cytotoxicity against cancer stem-like cells, particularly in glioblastoma and triple-negative breast cancer models. The compound, upon deacetylation, yields an active metabolite—4,4'-dihydroxydiphenyl-2-pyridyl-methane (DDPM)—which exhibits potent anti-proliferative effects. The diphenylmethane core and hydroxyl functional groups play a critical role in modulating its anticancer activity. In xenograft models, bisacodyl derivatives have demonstrated the ability to reduce tumor size and prevent recurrence, especially in chemoresistant phenotypes. The pharmacokinetics of Bisacumol support its use as a low-toxicity candidate, primarily metabolized in the gut with minimal systemic absorption. This selective activation profile could allow targeted cancer therapy with reduced side effects. The ability to repurpose an FDA-approved drug with a well-characterized safety profile adds immense value to translational oncology. Hence, our molecular docking and structural evaluation of Bisacumol align with emerging literature suggesting its utility beyond conventional use, positioning it as a dual-function therapeutic candidate.

While these findings are encouraging, several limitations of our study warrant mention. First, in vitro and in silico results require validation through cellular and animal models to establish clinical relevance. Second, the use of computational prediction tools, while efficient, carries a degree of uncertainty that must be offset by experimental corroboration. Lastly, phytocompound interactions with multiple targets and off-target effects remain unexplored and should be addressed in future studies to refine therapeutic precision.

CONCLUSION

This multidisciplinary investigation highlights the therapeutic promise of *Curcuma longa* and its phytoconstituents, particularly Bisacumol, as a potential anticancer agent against NSCLC. The integration of nanoparticle formulation, antioxidant and antimicrobial evaluation, and in silico approaches creates a comprehensive framework for identifying bioactive candidates with translational value. Rather than focusing solely on experimental metrics, this study emphasizes the future scope of phytocompound-based interventions, particularly those enhanced via nanotechnology, in overcoming limitations associated with synthetic chemotherapeutics. The virtual screening and ADMET profiling ensured pharmacological feasibility while minimizing the risk of false positives, making the proposed candidate a strong contender for preclinical evaluation. Although limited by the absence of in vivo validation, the structural and pharmacodynamic insights offer a strong foundation for hypothesis-driven translational research.

References

- [1] Alduais Y, Zhang H, Fan F, Chen J, Chen B. Non-small cell lung cancer (NSCLC): A review of risk factors, diagnosis, and treatment. Medicine (Baltimore). 2023; 102(8):e32899.
- [2] Deshpand R, Chandra M, Rauthan A. Evolving trends in lung cancer: Epidemiology, diagnosis, and management: Epidemiology, diagnosis, and management. Indian J Cancer. 2022;59(Supplement):S90–105.

- [3] Singh N, Agrawal S, Jiwnani S, Khosla D, Malik PS, Mohan A, et al. Lung cancer in India. J Thorac Oncol. 2021;16(8):1250-66
- [4] Kratzer TB, Bandi P, Freedman ND, Smith RA, Travis WD, Jemal A, et al. Lung cancer statistics, 2023. Cancer . 2024;130(8):1330–48.
- [5] Yang Y, Li N, Wang T-M, Di L. Natural products with activity against lung cancer: A review focusing on the tumor microenvironment. Int J Mol Sci. 2021;22(19):10827.
- [6] Amatto P de PG, Chaves L, França S de C, Carvalho JCT, Carmona F, Pereira AMS. Efficacy of different pharmaceutical forms of Curcuma longa or curcumin in reducing oral mucositis severity and incidence in cancer patients: a systematic review and meta-analysis. Front Pharmacol. 2025;16:1560729.
- [7] Jyotirmayee B, Mahalik G. A review on selected pharmacological activities of Curcuma longa L. International Journal of Food Properties. 2022;25(1):1377–98.
- [8] Ombredane AS, Silva VRP, Andrade LR, Pinheiro WO, Simonelly M, Oliveira JV, et al. In vivo efficacy and toxicity of curcumin nanoparticles in breast cancer treatment: A systematic review. Front Oncol. 2021;11:612903.
- [9] Jain A, Jain P, Soni P, Tiwari A, Tiwari SP. Design and characterization of silver nanoparticles of different species of Curcuma in the treatment of cancer using human colon cancer cell line (HT-29). J Gastrointest Cancer. 2023;54(1):90–5.
- [10] Bontzolis CD, Dimitrellou D, Plioni I, Kandylis P, Soupioni M, Koutinas AA, et al. Effect of solvents on aniseed aerial plant extraction using soxhlet and ultrasound methods, regarding antimicrobial activity and total phenolic content. Food Chem Adv. 2024;4(100609):100609.
- [11] Alharbi NS, Alsubhi NS, Felimban AI. Green synthesis of silver nanoparticles using medicinal plants: Characterization and application. J Radiat Res Appl Sci. 2022;15(3):109–24.
- [12] Naveed M, Bukhari B, Aziz T, Zaib S, Mansoor MA, Khan AA, et al. Green synthesis of silver nanoparticles using the plant extract of Acer oblongifolium and study of its antibacterial and antiproliferative activity via mathematical approaches. Molecules. 2022;27(13):4226.
- [13] Flieger J, Franus W, Panek R, Szymańska-Chargot M, Flieger W, Flieger M, et al. Green synthesis of silver nanoparticles using natural extracts with proven antioxidant activity. Molecules. 2021;26(16):4986.
- [14] Sharaf MH, Abdelaziz AM, Kalaba MH, Radwan AA, Hashem AH. Antimicrobial, antioxidant, cytotoxic activities and phytochemical analysis of fungal endophytes isolated from Ocimum Basilicum. Appl Biochem Biotechnol. 2022;194(3):1271–89.
- [15] Vivek-Ananth RP, Mohanraj K, Sahoo AK, Samal A. IMPPAT 2.0: An enhanced and expanded phytochemical atlas of Indian medicinal plants. ACS Omega. 2023;8(9):8827–45.
- [16] Karatzas E, Zamora JE, Athanasiadis E, Dellis D, Cournia Z, Spyrou GM. ChemBioServer 2.0: an advanced web server for filtering, clustering and networking of chemical compounds facilitating both drug discovery and repurposing. Bioinformatics. 2020;36(8):2602–4.
- [17] Galgale S, Zainab R, Kumar A. P, Nithya, Susha, Sharma S. Molecular docking and dynamic simulation-based screening identifies inhibitors of targeted SARS-CoV-2 3clpro and human ace2. Int J Appl Pharm. 2023;297–308.
- [18] Li Y, Yan B, He S. Advances and challenges in the treatment of lung cancer. Biomed Pharmacother. 2023;169(115891):115891.
- [19] Xu J, Tian L, Qi W, Lv Q, Wang T. Advancements in NSCLC: From pathophysiological insights to targeted treatments: From pathophysiological insights to targeted treatments. Am J Clin Oncol. 2024;47(6):291–303.
- [20] Das PS. A review on computer aided drug design in drug discovery. World J Pharm Pharm Sci. 2017;279–91.
- [21] Aghebati-Maleki A, Dolati S, Ahmadi M, Baghbanzhadeh A, Asadi M, Fotouhi A, et al. Nanoparticles and cancer therapy: Perspectives for application of nanoparticles in the treatment of cancers. J Cell Physiol. 2020;235(3):1962–72.
- [22] Miquel J, Bernd A, Sempere JM, Díaz-Alperi J, Ramírez A. The curcuma antioxidants: pharmacological effects and prospects for future clinical use. A review. Arch Gerontol Geriatr. 2002;34(1):37–46.
- [23] Verma RK, Kumari P, Maurya RK, Kumar V, Verma RB, Singh RK. Medicinal properties of turmeric (Curcuma longa L.): A review. Int J Chem Stud. 2018;6(4):1354–7.
- [24] Kaur T, Madgulkar A, Bhalekar M, Asgaonkar K. Molecular docking in formulation and development. Curr Drug Discov Technol. 2019;16(1):30–9.